Deep learning enhanced ALPS reveals genetic and environmental factors of brain glymphatic function

Cha Lin,[a,b,e] Hao Wu,[a,b,e] Wenbiao Xian,[c] Yifan Zheng,[c] Wenxuan Du,[a,b] Xinyi Chen,[a,b] Jinxia Li,[a,b] Weineng Chen,[c] Lishan Lin,[c] Fengjuan Su,[c] Zhong Pei,[c] and Ganqiang Liu,[a,b,d,*] For The Alzheimer's Disease Neuroimaging Initiative, and For The European Prevention of Alzheimer's Disease (EPAD) Consortium

[a]Shenzhen Key Laboratory of Systems Medicine in Inflammatory Diseases, School of Medicine, Shenzhen Campus of Sun Yat-sen University, Shenzhen, Guangdong, 518107, China
[b]Department of Medical Informatics and Neurobiology Research Center, School of Medicine, Shenzhen Campus of Sun Yat-sen University, Shenzhen, Guangdong, 518107, China
[c]Department of Neurology, The First Affiliated Hospital, Sun Yat-sen University; Guangdong Provincial Key Laboratory of Diagnosis and Treatment of Major Neurological Diseases, National Key Clinical Department and Key Discipline of Neurology, Guangzhou, 510080, China
[d]Guangdong Province Key Laboratory of Brain Function and Disease, Guangzhou, 510080, China

eBioMedicine
2026;124: 106133
Published Online xxx
https://doi.org/10.1016/j.ebiom.2026.106133

Summary

Background The glymphatic system plays a critical role in brain waste clearance and health. Diffusion tensor imaging along the perivascular space (DTI-ALPS) is an emerging approach to assess glymphatic function, but manual analysis is limited by its subjectivity and laboriousness in clinical practice. To address these challenges, we developed a deep learning-enhanced DTI-ALPS (dALPS) method that automates and enhances measurement of DTI-ALPS in large-scale cohorts, enabling us to uncover its genetic and environmental determinants.

Methods We proposed an automated workflow combining convolutional neural network (CNN) and You Only Look Once (YOLO) for region-of-interest detection in DTI images. Using this method, we calculated dALPS index for over 65,000 participants from UK Biobank and multiple cohorts, and performed a genome-wide association study (GWAS). Additionally, we conducted transcriptome-wide association study (TWAS) and proteome-wide association study (PWAS) to explore the genetic and molecular underpinnings of glymphatic function. Associations between dALPS and demographic, lifestyle, and clinical traits were comprehensively evaluated. Mediation analysis was conducted to explore the potential mediating role of pharmacological treatments, including antidepressants and sleep medications, in the relationship between disease status and dALPS outcomes.

Findings Our automated dALPS index showed excellent reliability and reproducibility compared to conventional manual techniques (intraclass correlation coefficient = 0·95). We observed that the dALPS index was associated with a wide range of body composition measures and brain structures across different age groups and sex. GWAS identified five significant genetic loci associated with dALPS, two of which were replicated in an independent dataset. Subsequent TWAS and PWAS analyses highlighted potential causal genes and proteins linked to brain fluid dynamics. We found that higher healthy lifestyle index (HLI) was positively correlated with improved dALPS, and confirmed the associations between reduced dALPS and various central nervous system (CNS) disorders, including depression, anxiety and neurodegenerative diseases. Notably, mediation analysis indicated that antidepressants were a risk factor for lower brain glymphatic function (P = 0·004) by partly mediating the risk factor of depression.

Interpretation The dALPS analysis provides a reliable, precise, and automated biomarker for assessing brain glymphatic function. Our findings illuminate the genetic and environmental determinants of glymphatic activity, underscoring the potential of dALPS in clinical assessment, disease prediction and targeted therapeutic strategies.

Funding G.L.'s work is supported by National Natural Science Foundation of China (No. 32470708, No. 32270701), Shenzhen Fundamental Research Program (JCYJ20240813151132042), Young Talent Recruitment Project of Guangdong (2019QN01Y139), Shenzhen Key Laboratory for Systems Medicine in Inflammatory Diseases (ZDSYS20220606100803007) and The Science and Technology Planning Project of Guangdong Province

*Corresponding author. School of Medicine, Shenzhen Campus of Sun Yat-sen University, No. 66, Gongchang Road Shenzhen, Guangdong, 518107, China.
E-mail address: liugq3@mail.sysu.edu.cn (G. Liu).
[e]These authors contributed equally to this work.

(2023B1212060018). Z.P.'s work is supported by National Natural Science Foundation of China (No. 82271266) and The Shenzhen Medical Research Fund (C2501030).

Keywords: DTI-ALPS; Glymphatic system; Deep learning; Genome-wide association study; Central nervous system disease

Research in context

Evidence before this study

The glymphatic system is essential for clearing brain waste, and the DTI-ALPS index has emerged as a non-invasive marker of its function. Numerous studies have linked reduced DTI-ALPS indexes to brain diseases, but they relied on manual or semi-automated ROI placement, limiting large-scale application. While previous genetic analyses revealed potential associations, deep learning-based methods and multi-omics integration remain underexplored in glymphatic imaging.

Added value of this study

This study provides a deep learning–enhanced DTI-ALPS (dALPS) method that enables automated and reliable measurement of glymphatic function. In our analysis of over 65,000 individuals, many genetic loci, causal genes and proteins, lifestyle factors, and associations with neuropsychiatric diseases were identified. These findings establish dALPS as a scalable biomarker and reveal insights into the genetic and environmental influences on brain waste clearance.

Implications of all the available evidence

This study suggests that dALPS index is a potential biomarker for early detection and monitoring of brain health, providing insights into preventive strategies and personalized interventions targeting brain clearance pathways.

Introduction

The glymphatic system plays a pivotal role in maintaining homeostasis by facilitating the clearance of metabolic waste,[1] including amyloid-beta and tau proteins, which are implicated in neurodegenerative diseases such as Alzheimer's disease (AD)[2] and Parkinson's disease (PD).[3] However, assessing the function of the glymphatic system in vivo poses a considerable challenge.[4,5] Slice-based fluorescent imaging following tracer injection into the cisternal cerebrospinal fluid (CSF) is the most commonly used method for evaluating glymphatic exchange.[1] Keil et al.[6] introduced a novel approach for real-time quantification by employing co-injection of infrared (IR) and conventional fixable fluorescent tracers in mice. Besides, Han et al.[7] proposed the global blood-oxygen-level-dependent signal–CSF coupling (gBOLD-CSF), which represents the coupling between the global functional magnetic resonance imaging (fMRI) signal and CSF influx, as a potential proxy for glymphatic function, demonstrating its correlation with AD-related pathology. Additionally, Harrison et al. utilized an ultra-long echo time, low b-value, multi-direction diffusion-weighted MRI sequence (DTI_{low-b}) to assess perivascular fluid movement in mice,[8] while Han et al. were the first to employ DTI_{low-b} to measure glymphatic system influx in humans.[9] Ringstad et al.[10] detected glymphatic clearance function directly by comparing magnetic resonance imaging (MRI) signal intensity before and after intrathecal injection of gadolinium. Although informative, many of these techniques are invasive or technically challenging, limiting their utility in large-scale human studies.

To overcome these limitations, Taoka et al.[11] introduced the Diffusion Tensor Imaging–Along the Perivascular Space (DTI-ALPS) index as a non-invasive and reliable approach for evaluating the human glymphatic system. The DTI-ALPS index leverages the assumption that water diffusivity along the perivascular spaces (PVS) reflects CSF–interstitial fluid (ISF) exchange, thereby serving as an indicator of glymphatic function. The DTI-ALPS index is calculated from the diffusion tensor model parameters in a region of interest (ROI) at the level of the lateral ventricles, where deep medullary veins run mainly in parallel with the image slice orientation (Fig. 1a). Reduced DTI-ALPS index has been reported in diverse neurological disorders, suggesting a broadly compromised glymphatic pathway. These include AD,[11] PD,[12,13] possible idiopathic rapid eye movement sleep behaviour disorder (piRBD),[13] multiple sclerosis,[14] stroke,[15] glioma,[16] and fibromyalgia,[17] suggesting DTI-ALPS as a widely used method for characterizing glymphatic dysfunction in clinical and research settings.

Conventionally, the calculation of the DTI-ALPS index has been performed manually, requiring skilled operators to identify and measure specific ROIs on a single slice. This process is time-consuming and prone to inter-operator variability, making it impractical for routine clinical visits or large-scale population studies.[18] To address these challenges, several automated

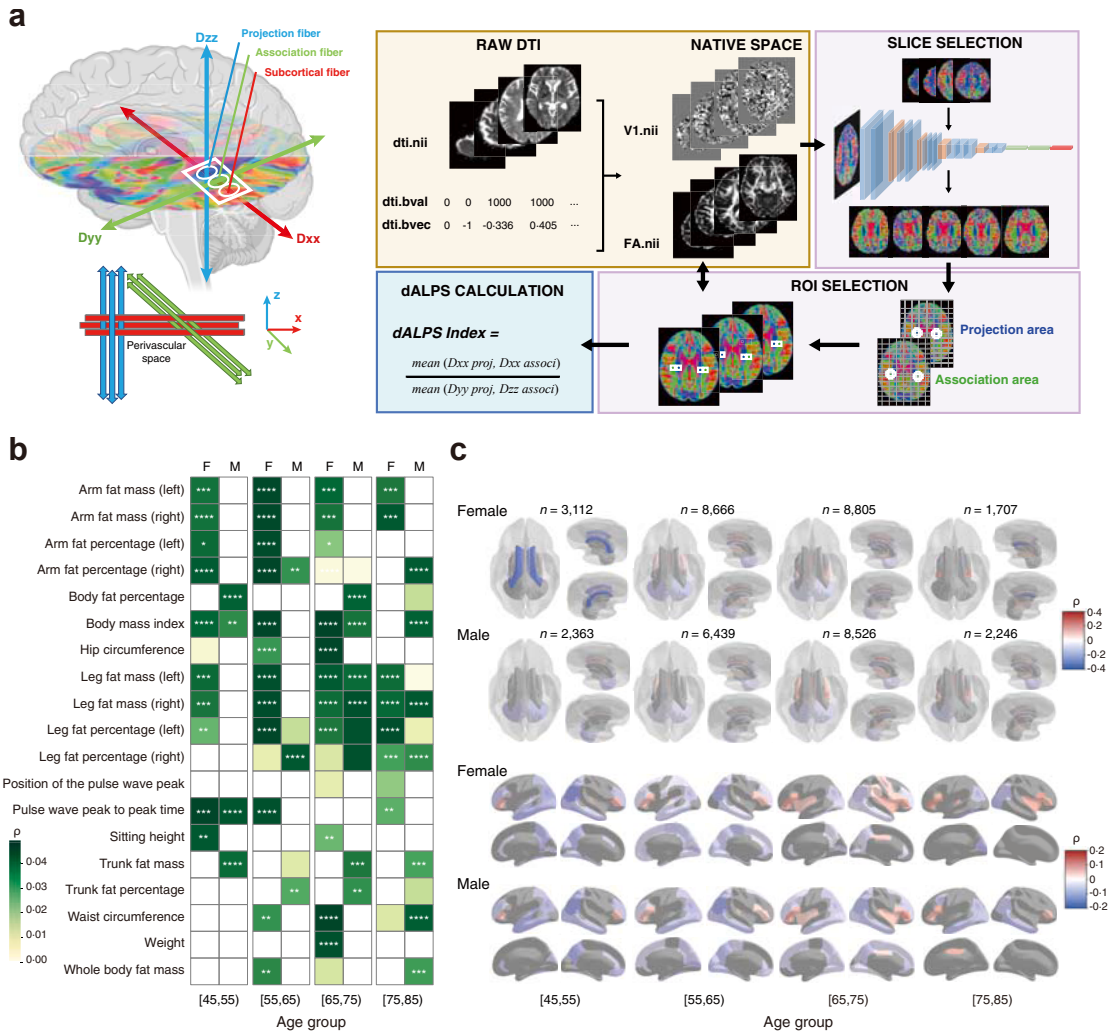

Fig. 1: **dALPS index and its association with body composition and brain structural changes.** (**a**) Schematic representation of DTI-ALPS index calculation. The left panel illustrates the DTI-ALPS method, showing projection, association, and subcortical fibers in relation to the perivascular space. The right panels depict the dALPS processing pipeline, including raw DTI data transformation into native space, slice selection, and region of interest (ROI) extraction. The dALPS index is calculated as the ratio of diffusion tensor components in projection versus association areas. (**b**) Heatmap of Spearman rank correlations (ρ) between the dALPS index and body-composition traits across age-by-sex strata; color encodes ρ, cells are colored only for nominal P-value < 0·05 (two-sided Spearman test), and asterisks denote significance after Benjamini–Hochberg FDR correction (q < 0·05). (**c**) Brain maps highlighted regions significantly correlated with dALPS in different age groups and sex. The upper panel focused on subcortical structures (FreeSurfer ASEG), while the lower panel presented cortical segmentations (FreeSurfer DKT).

approaches have been developed. For instance, Tatekawa et al.[19] introduced a method that registered vector images to a standard space and created reoriented diffusivity maps, significantly improving reproducibility in calculating the ALPS index. Similarly, Liu et al.[20] and Ran et al.[21] automated the DTI-ALPS calculation by predefining the center coordinates of ROIs in the JHU-ICBM FA template and co-registering each subject's FA map to the template, facilitating consistent ROI placement across subjects and enhancing the efficiency and scalability of the analysis. Additionally, Huang et al.[22] developed a method involving the creation of group-averaged ROI templates by randomly selecting participants from large cohorts to generate an average ROI template from the training set. These advancements have significantly enhanced the reproducibility and scalability of DTI-ALPS calculations, facilitating large-scale analyses of the function of the human glymphatic system. Huang et al.[22] analyzed over 30,000 individuals from the UKB and identified hundreds of genetic loci significantly associated with the DTI-ALPS index, further pinpointing 161 genes related to the DTI-ALPS index. Additionally, genetic correlation analyses confirmed a shared underlying genetic mechanism

linking the DTI-ALPS index, ventricular volume, and CSF tau levels.[22] Ran et al.[21] identified 17 genetic loci associated with regional DTI-ALPS index in around 40,000 individuals, and indicated that a lower DTI-ALPS index was a risk factor for ischemic stroke.

In this study, we advanced DTI-ALPS analysis by developing a deep learning–enhanced framework that can easily be deployed (Fig. 1a). Using a diverse training set of DTI images from several hundred Chinese and European participants, we established a robust deep learning-based tool capable of accurately identifying multi-slice ROIs and computing a refined deep learning–enhanced DTI-ALPS index (dALPS). Applying this pipeline, we successfully derived the dALPS index from over 65,000 participants from UK Biobank and multiple cohorts, and performed comprehensive downstream analyses. Our results provide insights into the genetic and environmental determinants of glymphatic system function, expanding our understanding of how glymphatic disruption may contribute to neurological and psychiatric diseases and offering an efficient, scalable protocol for high-throughput glymphatic assessment in large cohorts.

Methods

Study participants

We utilized MRI imaging and genetic data from participants in multiple cohorts: Guangzhou Healthy Aging and Dementia Cohort (GHAD), Guangzhou Precision Medicine Parkinson's Cohort (GPMP), Alzheimer's Disease Neuroimaging Initiative 3 (ADNI3), Parkinson's Progression Markers Initiative (PPMI), UK Biobank (UKB), Open Access Series of Imaging Studies 3 (OASIS3) and European Prevention of Alzheimer's Dementia Longitudinal Cohort Study (EPAD LCS V.IMI, https://doi.org/10.34688/epadlcs_v.imi_20.10.30). The demographic and clinical characteristics of the subjects at baseline from each cohort are summarized in Table 1. For cohorts with longitudinal designs, only one imaging time point per participant was used as specified below; repeated scans were not included in primary analyses.

DTI acquisition and pre-processing

DTI imaging was performed using a single-shot echo planar imaging sequence. For the GHAD cohort, scanning was carried out on a Siemens Prisma scanner, while the GPMP cohort was scanned on a Siemens Verio scanner. DTI images for other cohorts, including PPMI, ADNI3, UKB, OASIS3, and EPAD LCS v.IMI, were obtained from their respective databases and platforms. Detailed DTI protocols are available in the Supplementary Methods. In addition, we provide a cohort-level protocol summary (Table S1), which details scanner manufacturer and model, field strength, repetition time (TR) and echo time (TE), in-plane resolution and slice thickness, diffusion weighting (b-values), number of diffusion-encoding directions, and the use of parallel imaging or multiband acceleration where applicable.

The DTI data were pre-processed using FMRIB Software Library (FSL, version 6·0). The pre-processing steps included: (1) conversion of DTI data from Digital Imaging and Communications in Medicine (DICOM) to Neuroimaging Informatics Technology Initiative (NIfTI) format; (2) correction for head motion and brain extraction using FSL's eddy_correct and bet tools; (3) fitting the diffusion tensor model with FSL's dtifit tool to obtain tensor parameters; and (4) segmentation of the tensor file into multiple 3D files using FSL's fslsplit tool. The diffusion tensor model's output was then transformed into a color-coded RGB map using the Python Imaging Library (PIL, version: 8·0·1, Supplementary Methods), with voxel values representing the direction of the primary eigenvector.

Development and workflow of dALPS

500 subjects with DTI images from GHAD and GPMP cohorts, and 500 from PPMI and ADNI3 cohorts were randomly selected. After pre-processing and conversion via dcm2png, V1 files in each DTI image were transformed into color-coded maps, yielding 106,278 color-coded maps from 1000 subjects. Among these, 2125 images were annotated 'yes' (lateral ventricle body slices), and the remaining 104,153 were annotated 'no' by two neurologists. For 'yes' images, the two neurologists

	GHAD	GPMP	ADNI3	PPMI	UK Biobank	OASIS3	EPAD
Sample size (*n*)	201	352	702	668	61,190	1026	1078
Age at MRI (mean years [SD])	67·48 (7·20)	64·26 (9·11)	74·35 (7·48)	63·46 (9·38)	54·46 (7·48)	49·65 (8·84)	64·50 (7·22)
Male (*n*, %)	80 (39·80)	250 (71·02)	330 (47·01)	392 (58·68)	28,989 (47·37)	468 (45·61)	465 (43·14)
Years of education (mean years [SD])	11·29 (3·24)	11·22 (5·10)	15·76 (2·39)	15·87 (3·41)	NA[b]	15·57 (2·76)	4·26 (3·73)
dALPS[a] (mean [SD])	1·129 (0·11)	1·198 (0·13)	1·115 (0·12)	1·124 (0·13)	1·189 (0·13)	1·105 (0·14)	1·173 (0·12)

GHAD, Guangzhou Healthy Aging and Dementia Cohort; GPMP, Guangzhou Precision Medicine Parkinson's Cohort; ADNI, Alzheimer's Disease Neuroimaging Initiative; PPMI, Parkinson's Progression Markers Initiative; OASIS, Open Access Series of Imaging Studies; EPAD, European Prevention of Alzheimer's Dementia Study; SD, Standard Deviation; NA, Not applicable. [a]dALPS is the dALPS index of the subject at the time of their first DTI screening during the study. [b]UK Biobank does not directly provide the exact number of years of education for each participant.

Table 1: **Demographic and clinical characteristics of participants across cohorts in this study.**

used LabelImg (version: 1·8·6) to annotate anchor boxes for projection and association fiber ROIs. To mitigate class imbalance and improve model robustness, we applied data augmentation to the positive ('yes') images, including random in-plane rotation (±15°) and horizontal translation (≤20% of the image width). This procedure expanded the 2125 original positive images to 9665 augmented positive images. Combined with the 104,153 negative images, the final dataset comprised 113,818 images. All images were resampled to 224 × 224 pixels. The dataset was randomly divided into training and validation sets (80–20) at the subject level. The validation set was used only for model selection and early stopping: convergence monitoring, learning rate/regularization tuning, and augmentation intensity adjustment within a pre-specified grid. Data augmentation was applied exclusively to the training set.

For slice classification, we used a lightweight Visual Geometry Group (VGG)-style CNN consisting of three convolutional blocks (32, 64, and 128 filters, each followed by max-pooling) and two fully connected layers (128 neurons). The model input size was 224 × 224 pixels. Training was performed using stochastic gradient descent (learning rate 0·001, momentum 0·9, batch size 32) for up to 50 epochs, with early stopping if validation loss plateaued. For ROI detection, we employed the YOLOv5s architecture with an input size of 640 × 640 pixels, batch size 50, and 300 epochs. Default YOLOv5 data augmentation strategies (color jitter, scaling, flipping, mosaic) were applied. Training was initialized with the yolov5s.pt weights, and the best model was selected based on validation loss. All hyperparameters and thresholds were finalized prior to any external evaluation. A full summary of model architectures and hyperparameters is provided in Table S2. ROIs were defined based on predefined color ranges. dALPS index was then computed for each ROI pair per subject. The term dALPS (deep learning–enhanced ALPS) is used to indicate that the original DTI-ALPS formula is preserved, with ROI placement automated via deep learning models. The relationship between manual DTI-ALPS and dALPS was validated by two neurologists. The detailed methods for the development of dALPS are available in the Supplementary Methods.

Inter-rater reliability and external testing of dALPS

To establish the reliability of manual DTI-ALPS as a reference standard and to validate the automated pipeline against an independent benchmark, we first quantified inter-rater consistency between two experienced neurologists across five cohorts (ADNI3, PPMI, UKB, OASIS3, EPAD; n = 200 subjects per cohort). For each subject, the raters independently placed ROIs and manually calculated DTI-ALPS, and agreement was evaluated using intraclass correlation coefficient (ICC, model A, 1), mean absolute error (MAE), Lin's concordance correlation coefficient (CCC), Pearson correlation, and Bland–Altman analysis in accordance with established guidelines; results are reported in Table S3 and illustrated in Fig. S7. To address potential overfitting and to provide an independent benchmark, we tested the dALPS pipeline on datasets that were not used in model development, with a primary independent test set drawn from the UKB and supplementary test cohorts from OASIS3 and EPAD. Specifically, we analyzed 1000 randomly selected UKB subjects as the main test set, and 200 subjects from OASIS3 and 200 from EPAD as supplementary confirmations. For each subject, two neurologists independently manually calculated DTI-ALPS index, which were averaged to form the manual reference. Automated dALPS index was computed using the proposed pipeline. Agreement between manual and automated index was quantified using ICC, MAE, Lin's CCC, Pearson correlation, and Bland–Altman analysis.

Cross-cohort stability analysis

To evaluate potential site-specific or cohort-related bias in dALPS index, we performed additional statistical analyses across the seven independent cohorts. First, we compared the distribution of ALPS index across cohorts using both a one-way analysis of variance (ANOVA) and a nonparametric Kruskal–Wallis test. Second, we fitted a linear mixed effects model (LMM) with cohort specified as a random intercept to partition the variance in dALPS into between-cohort and within-cohort components. From this model, we estimated the variance attributable to cohort-level effects, the residual within-cohort variance, and the ICC to quantify the proportion of total variability explained by cohort membership. Boxplots/violin plots of cross-cohort distributions and a bar plot of variance components are shown in Fig. S10.

Genetic data processing

Genotyping and imputation were performed by the UKB team.[23] We acquired the imputed genotype data from the UKB (Data-Field 22828). To minimize confounding from population stratification, we selected only those UKB participants who both self-identified as 'White British' and clustered closely with the European reference samples in a principal component analysis. Subsequently, we used PLINK (version: 2·0; a whole–genome association analysis toolset)[24] to perform further quality control. The detailed quality control procedures are provided in the Supplementary Methods. Finally, we retained 53,719 individuals and 7,906,415 autosomal single nucleotide polymorphisms (SNPs; hg19). Furthermore, we integrated the EPAD, ADNI, and PPMI cohorts to form an independent validation set: after applying a quality control

pipeline identical to that used for the UKB data, 1596 individuals and 7,316,787 SNPs (hg38) were retained.

dALPS index GWAS

We performed genome-wide association study (GWAS) on the dALPS index (mean values) for the discovery dataset, replication dataset, combined dataset and independent validation set using the fast MLM-based genome-wide association tool (fastGWA)[25] implemented in Genome-wide Complex Trait Analysis (GCTA, version: 1·94·1).[26] This method utilizes a sparse genetic relationship matrix (sparse GRM) to account for both population structure and kinship, allowing for the inclusion of related individuals to enhance statistical power. We adjusted the model for age, age^2, sex, imaging center, genotype array, systolic blood pressure, and the top 40 genetic principal components (PCs). For the discovery and combined datasets, the GWAS significance threshold was set at *P*-value $<5 \times 10^{-8}$, whereas for the replication dataset, a significance threshold of *P*-value <0·05 was applied. In the independent validation set, we performed the GWAS analysis adjusting for age, age^2, sex, cohort, and the top 40 PCs. Associations with *P*-value <0·05 were considered successfully validated. For downstream analyses, summary statistics from the combined dataset were used by default. Additionally, we performed joint association analysis (GCTA-COJO)[27] using default parameters in GCTA to identify independent genetic variants at significant loci. We also calculated the genomic inflation factor (λ) and the intercept of linkage disequilibrium score regression (LDSC, version: 1·0·1)[28] to assess whether population structure was adequately controlled in the GWAS. LDSC reference LD files were derived from the European population in the 1000 Genomes Project (https://doi.org/10.5281/zenodo.7768714).

Transcriptome- and proteome-wide association studies

PrediXcan[29] and MR-JTI (joint-tissue imputation (JTI) and Mendelian randomization framework)[30] were used to perform transcriptome-wide association study (TWAS). We next performed causal inference using the MR-JTI.r function. We performed a proteome-wide association study (PWAS) to assess the association between protein expression and dALPS index using the FUSION software.[31] The genetic effect weights for protein expression were derived from Wingo et al.[32] Based on the GWAS summary statistics from the independent validation set, we performed a replication analysis for the significant TWAS/PWAS genes/proteins using the same method. Associations with *P*-value <0·05 were considered successfully validated. Subsequently, we performed summary data-based Mendelian Randomization (SMR)[33] to identify potential causal proteins. Detailed TWAS and PWAS are provided in the Supplementary Methods. Furthermore, to test whether the significant associations for genes/proteins identified by TWAS/PWAS were driven by the same causal variants as the GWAS signals for the dALPS index, we performed colocalization analysis using the coloc tool (version: 5·2·3).[34]

Cell-type enrichment analysis

We performed a cell-type enrichment analysis using the scDRS tool[35] to test for associations between specific cell types and the dALPS index. This analysis utilized a single-nucleus RNA-sequencing (snRNA-seq) dataset from healthy subjects in the Accelerating Medicines Partnership Parkinson's Disease (AMP-PD) cohort, for which the quality control and cell-type annotation procedures were detailed in our prior work.[36] The scDRS method integrates GWAS summary statistics with snRNA-seq data to assess whether trait-associated genes are preferentially expressed in certain cell types. Further details on the single-cell quality control (QC) and annotation are described in the Supplementary Materials.

Statistical analyses

All statistical analyses in this study were performed using R (version: 4·1·0; https://CRAN.R-project.org/). All analyses involving UKB's raw imaging data and genomic data were conducted on the DNAnexus platform using JupyterLab, with the IMAGE_PROCESSING feature selected. Analyses involving EPAD's genomic and clinical data were carried out on the Alzheimer's Disease Data Initiative (ADDI) workspace virtual machine. Full details on the statistical methods, including the analysis of brain volumes, GWAS locus annotation, heritability estimation, genetic correlations, body composition and lifestyle factors, CNS disorders, case–control matching, and mediation analysis, are presented in the Supplementary Methods.

Although several cohorts are longitudinal studies, all primary analyses in this study were conducted using a single imaging time point per participant. For model development, we used baseline DTI scans only (GHAD, GPMP, PPMI, ADNI3). For independent validation, we used the first available imaging assessment per subject: UKB (Instance 2 imaging visit), OASIS3 (first DTI session), and EPAD (first DTI session). For association analyses (e.g., structural MRI metrics, HLI, lifestyle/environmental measures), covariates were drawn from the same visit window as the dALPS measurement (UKB Instance 2 for imaging-based analyses). For disease-risk analyses, dALPS from the first imaging visit served as the exposure and incident diagnoses during follow-up as outcomes. If multiple DTI acquisitions existed within the same visit (e.g., rescans), we retained one acquisition according to a pre-specified QC rule (QC-pass and earliest acquisition). No repeated measures from the same participant were included in model development, validation, or primary association analyses.

To quantify the association between age and dALPS, we modeled age as a continuous predictor and fitted ordinary least-squares (OLS) regressions with (i) z-scored age to report the standardized slope β per 1 standard deviation (SD) of age, and (ii) age scaled in decades to report the absolute Δ per 10 years. For both metrics, we provide 95% confidence intervals (CIs) from Wald theory and from nonparametric bootstrap (2000 resamples). To convey practical relevance beyond *P*-values, we report the partial R^2 for age (computed from the age *t*-statistic) as the proportion of variance uniquely explained by age after the intercept. Potential nonlinearity was evaluated with restricted cubic splines (natural splines; 3 df) and a global Wald/ANOVA test comparing the spline model against the linear model; a small *P*-value indicates improved fit by allowing curvature. As a complementary, distribution-aware summary, we also present scatter/loess visualizations in the Supplement (figure referenced in the Results). For sex differences, we stratified the cohort into four age bins (45–54, 55–64, 65–74, 75–84 years) and compared females versus males within each bin. Effect sizes are reported as Cohen's *d* (female–male) with 95% bootstrap CIs (2000 resamples). Mean differences were additionally tested with Welch's *t*-test, and multiple testing across the four bins was controlled using Benjamini–Hochberg False Discovery Rate (FDR; we display *q*-values and significance stars in the figure). As a sensitivity analysis that removes any residual age imbalance inside bins, we fitted OLS models dALPS ~ sex + age within each age bin and standardized the sex coefficient by the within-bin pooled SD to obtain age-adjusted standardized contrasts with 95% CIs. For body composition features, we fitted OLS models of the form. We report standardized regression slopes (β per 1 SD of the feature), 95% confidence intervals (Wald and bootstrap, 2000 resamples), and partial R^2 values computed from the feature *t*-statistic. To quantify effect size beyond *P*-values, we also provide Cohen's f^2 (partial R^2/(1-partial R^2)). To evaluate correlations between dALPS and brain volumetric measures, we computed Spearman's correlation (ρ) between dALPS and each structural volume within each stratum. Stratum-specific ρ values were then pooled using random-effects meta-analysis (DerSimonian–Laird, Fisher *z* domain) to obtain an overall correlation with 95% CI and heterogeneity (I^2). Left and right hemisphere structures were merged when appropriate by inverse-variance weighting.

We evaluated whether medication use mediates the association between depression or other anxiety disorders and the dALPS index. Exposures and mediators were binary (yes/no), and the outcome (dALPS) was continuous. The primary analysis used a two-model framework with a linear probability model (LPM) for the mediator and a linear regression for the outcome. All models were adjusted for age, sex, and imaging site (fixed effects). Mediation effects—average causal mediation effect (ACME), average direct effect (ADE), total effect, and proportion mediated—were estimated with the R package 'mediation' (version 4·5·0) using quasi-Bayesian Monte Carlo (1000 simulations) to obtain 95% confidence intervals and two-sided *P*-values. For exploratory, class-specific analyses restricted to antidepressant classes with adequate sample size (Selective Serotonin Reuptake Inhibitors [SSRIs], Tricyclic Antidepressants [TCAs], Serotonin–Norepinephrine Reuptake Inhibitors [SNRIs], and Noradrenergic and Specific Serotonergic Antidepressants [NaSSAs]), we controlled the false discovery rate using Benjamini–Hochberg (FDR, threshold $q < 0{\cdot}10$). Model fit was summarized by R^2/adjusted R^2 and AIC/BIC for outcome models. Robustness to unmeasured mediator–outcome confounding was examined via medsens, replication in the EPAD cohort followed the same analysis. We provide a schematic directed acyclic graph (DAG) for illustrating the analysis in this study (Figs. S24 and S25).

Role of funders

The funders of the current study had no role in the design, data collection, data analysis, data interpretation, or writing of this manuscript.

Results

Development of deep learning enhanced DTI-ALPS (dALPS)

The dALPS workflow follows the conventional DTI-ALPS pipeline—DTI pre-processing, ROI selection, mask binarization, value extraction, and DTI-ALPS computation—but replaces manual ROI placement with a two-step deep learning approach (Fig. 1a, Supplementary Methods). Instead of using template-based ROI coordinates, our method uses a CNN to detect relevant DTI slices covering the lateral ventricles (typically 3–6 slices) and YOLOv5 to identify ROI positions. The CNN, trained with an 80/20 train-validation split, achieved high accuracy: AUC of 0·989 (95% CI: 0·946–0·992) and PRC of 0·883 (95% CI: 0·874–0·893) on validation data (Fig. S1a and b). This enables broader slice coverage compared to the single-slice focus of the conventional method.

We annotated the ROIs using labelImg and trained YOLOv5, which showed steadily improving loss functions (Fig. S2a–c f and g, f and g), and increasing precision, recall, and mean average precision (mAP) during training (Fig. S3d and e, i and j). YOLOv5 reached a mAP of 0·993 at an intersection over union (IoU) threshold of 0·5 (Fig. S3b), with high F1 score near 0·99 across all classes (Fig. S3c). Confusion matrix results showed robust classification (Fig. S4a), and model predictions were consistent across batches (Fig. S4). Detected objects similarity in location and

size was confirmed via correlogram analysis (Fig. S5). After object detection, two parallel ROIs were segmented (Fig. S6), and individual dALPS indexes were calculated by averaging left and right DTI-ALPS index.

Reliability of dALPS and its generalizability across cohorts

Despite extensive training and standardized instructions, manual DTI-ALPS presented moderate agreement between the two neurologists, with ICC values ranging from 0·29 to 0·62 across cohorts and Pearson correlations of 0·29–0·62 (all *P*-values <0·0001, Table S3 and Fig. S7). This finding underscores that even the manual method—widely regarded as the "gold standard"—is inherently subject to inter-rater variability. When validated against independent test sets, dALPS presented better agreement with manual DTI-ALPS, consistently outperforming inter-rater reliability between the two neurologists. In the UKB cohort (n = 1000), the automated index achieved ICC = 0·90, CCC = 0·90, MAE = 0·047, and Pearson r = 0·74 (*P*-value <0·0001, Table S4, Fig. S8). Comparable results were obtained in OASIS3 (n = 200, ICC = 0·80, r = 0·77) and EPAD (n = 200, ICC = 0·78, r = 0·80), details in Table S4, Fig. S9. Together, we showed that dALPS achieves reliability that is at least comparable to, and in some cases exceeds, the reproducibility of manual DTI-ALPS.

Given that the study draws on seven neuroimaging cohorts with different acquisition protocols, we further assessed the extent to which cohort membership influenced dALPS index. Distributional comparisons revealed significant differences in absolute value distributions across cohorts (Kruskal–Wallis test: H = 1703·2, *P*-value <0·0001; one-way ANOVA: F = 277·8, *P*-value <0·0001; Fig. S10a). To quantify the contribution of cohort-level variability, we applied a LMM with cohort specified as a random effect. The variance attributable to between-cohort differences was 0·00132, while within-cohort variance was 0·0177, corresponding to an ICC of 0·069. Thus, about 7% of the total variance in dALPS index could be explained by cohort membership (Fig. S10b).

dALPS index associated with demographics and brain structures

In the UK Biobank cohort (n = 61,011), the dALPS index showed a unimodal distribution (median 1·179; Q1 = 1·097, Q3 = 1·270; Fig. S11a). Age was associated with a small but consistent decline in dALPS: the standardized effect was β_std (per 1 SD age) = –0·020 (95% CI -0·0214 to –0·0193), with partial R^2 = 0·023 (Table S5). Sex differences were small in magnitude yet stable across age bins: Cohen's d (female–male) ≈ 0·22–0·31 (Table S6, Fig. S11b–c). Across other six independent datasets, the meta-analytic pooled difference was Hedges' g = 0·33 (95% CI 0·25–0·40; $I^2 \approx 0\%$), indicating a small but highly consistent effect (female higher than male, Table S7, Fig. S12g).

In addition, the dALPS index showed consistent associations with body-composition metrics, particularly adiposity-related measures such as leg, arm, trunk, and whole-body fat mass and percentage (Fig. 1b; Tables S8 and S9). Across age- and sex-stratified models, these associations were directionally uniform and generally positive, with effect sizes that were small in magnitude (median β_std ≈ 0·03; median partial $R^2 \approx 0{\cdot}1\%$). The strongest associations were observed for leg fat percentage (β_std ≈ 0·08–0·09; partial $R^2 \approx 0{\cdot}2\%$), followed by body fat percentage and trunk/arm fat percentage. Although the pulse-wave traits showed little to no association, the consistent pattern across multiple adiposity metrics suggests that higher fat composition is reliably linked to variation in dALPS.

We next examined brain structural measures. Effect sizes were summarized by Spearman correlation coefficients (ρ) with 95% CIs and pooled across the eight age-by-sex strata using random-effects meta-analysis. Ventricular/CSF and choroid-plexus measures showed the largest—yet small-to-moderate—associations with dALPS: VentricleChoroid ρ = –0·300 (95% CI –0·346 to –0·252; $\rho^2 \approx 9\%$), choroid-plexus ρ = –0·229 (–0·248 to –0·209; ~5%), CSF (whole brain) ρ = –0·169 (–0·193 to –0·146; ~3%), and WM-hypointensities ρ = –0·167 (–0·200 to –0·133; ~0·8%). In contrast, global/cortical measures were small (e.g., BrainSeg/SupraTentorial $\rho \approx -0{\cdot}08$, $\rho^2 \approx 0{\cdot}7\%$; Cortex $\rho \approx -0{\cdot}046$, $\rho^2 \approx 0{\cdot}2\%$) (Fig. S13). Full pooled estimates with heterogeneity (I^2) and FDR-adjusted *P*-values are provided in Table S10. Region-wise cortical maps (Fig. 1c) show predominantly negative correlations in parietal, temporal, precuneus, and pericalcarine regions, and positive correlations in pars orbitalis, pars triangularis, insula, pars opercularis, and posterior cingulate cortex, while ventricular structures (lateral, inferior lateral, third, and fourth ventricles) showed negative associations consistent with glymphatic function coupling to ventricular expansion and CSF homeostasis.

Identification of genome-wide association loci associated with dALPS index

Following rigorous QC procedures, we performed a GWAS on the mean dALPS index. In the discovery dataset (n = 37,543), we identified 24 significant SNPs (*P*-value < 5×10^{-8}, Table S11), four of which (rs12146713, rs12370774, rs7225002, rs2696466) were verified in the replication dataset (n = 16,176, *P*-value < 0·05, Table S11). Subsequent analysis of the combined dataset (n = 53,719) identified 34 significant SNPs (*P*-value < 5×10^{-8}, Fig. 2a, Table S11), with all four verified SNPs remaining significant (Table S11). We then performed COJO analysis on these 34 SNPs, identifying five lead SNPs: rs696859, rs12146713,

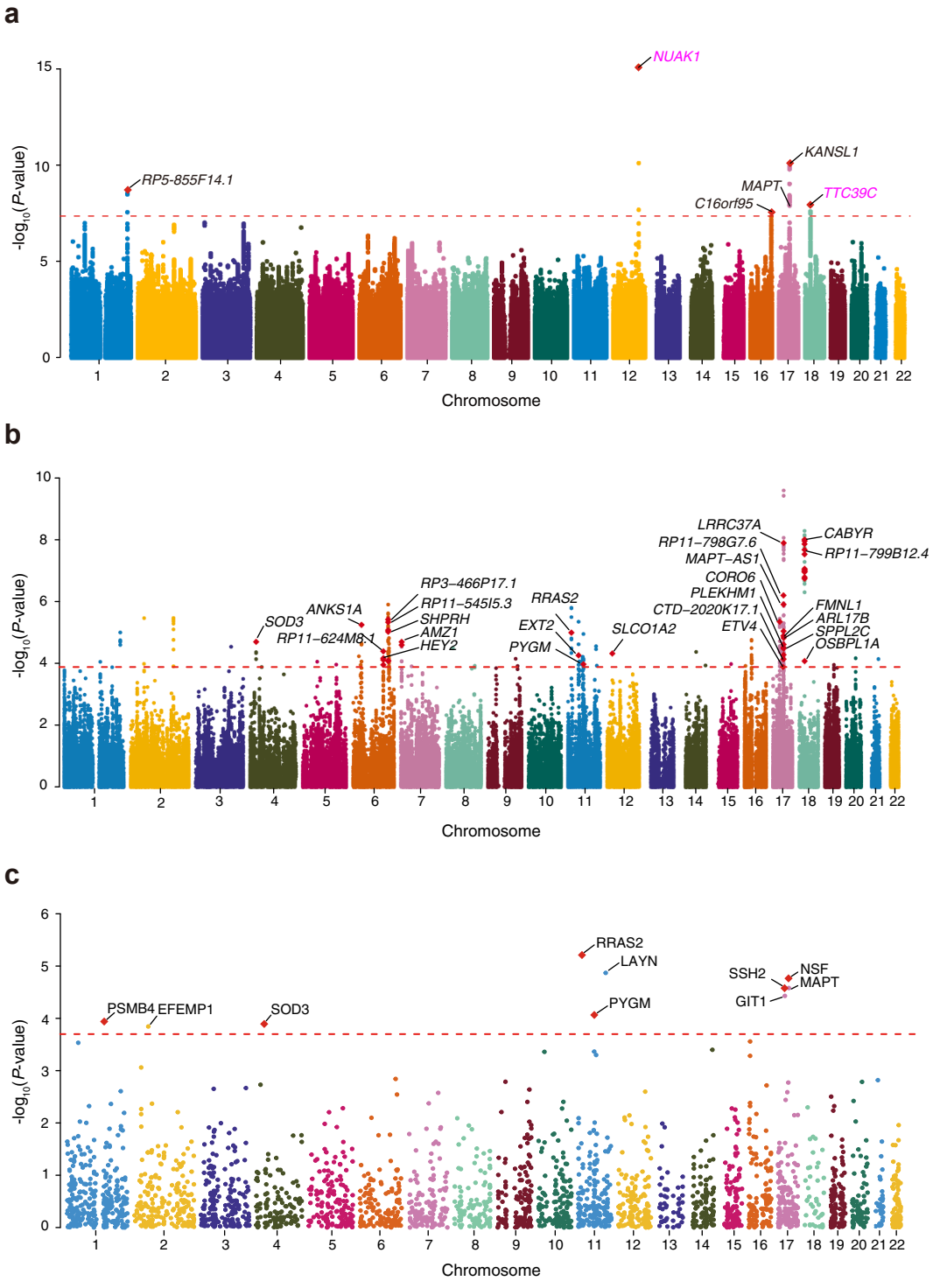

Fig. 2: **Manhattan plots of GWAS, TWAS and PWAS results for the mean dALPS index.** (**a**) Manhattan plot of GWAS results for the mean dALPS index in the combined UKB cohort (n = 53,719). The y-axis shows -$\log_{10}$ (P-value) for each SNP, and the x-axis shows the chromosomal base-pair position. P-values are two-tailed. The GWAS significance threshold (P-value < 5×10^{-8}) is indicated by a red dashed line. Lead SNPs are marked with red diamonds. Annotated genes for significant loci are labeled only at the most significant SNP. The lead SNPs validated in the independent dataset are labeled with their associated gene in magenta. (**b**) Manhattan plot of TWAS results across 13 brain tissues and whole blood. Each point represents a gene–tissue pair. The y-axis shows -$\log_{10}$ (P-value), and the x-axis displays the chromosomal position of

rs7225002, rs8083625, and rs4843555 (Fig. S14b–f, Table S11). Despite a genomic inflation factor (λ) of 1·099 in the combined dataset GWAS, the linkage disequilibrium score regression (LDSC) intercept was 1·0018 (SE = 0·0077), indicating effective control of population stratification. Subsequently, five significant loci were validated (*P*-value <0·05) in the GWAS analysis of an independent validation set, including two lead SNPs (rs12146713 and rs8083625, Fig. 2a, Table S11). The genomic inflation factor (λ) for the validation GWAS was 0·983, and the LDSC intercept was 0·9774 (SE = 0·0065).

Additionally, SNP-based heritability estimates for dALPS index were 13·4% using LDSC[28] and 31·2% using GCTA-GREML,[37] suggesting a partial genetic contribution. We subsequently annotated the significant loci using the Functional Mapping and Annotation (FUMA) platform, revealing that most were located in intronic and intergenic regions (Table S11). Specifically, the lead variant rs696859 was mapped to the intergenic region of *RP5-855F14·1*, rs12146713 located in the intronic region of NUAK family SNF1-like kinase 1 (*NUAK1*), rs4843555 located in the intergenic region near the *C16orf95* gene, rs7225002 located in the intronic region of KAT8 regulatory NSL complex subunit 1 (*KANSL1*), and rs8083625 located in the intronic region of Tetratricopeptide repeat domain 39C (*TTC39C*, Fig. 2a, Table S11). We performed a functional annotation of our five lead SNPs using HaploReg, and revealed that these variants are located in regions enriched with histone marks characteristic of active regulatory elements in brain tissues (including H3K4me1, H3K4me3, H3K27ac, and H3K9ac), suggesting they have a high potential to be functional (Table S12).

We also investigated the global/local genetic correlations between the dALPS index and 36 phenotypes spanning neuropsychiatric traits, sleep-related features, neurological diseases, metabolic disorders, cardiovascular traits and neuroimaging markers (Supplementary Methods, Table S14). Significant global genetic correlations (FDR <0·05) were observed between the dALPS index and body mass index (BMI, r_g = 0·095), snoring (r_g = 0·097), anxiety disorders (AND, r_g = 0·122), and mean diffusivity (MD, r_g = –0·189, Fig. S15a, Table S15). We observed 74 significant local genetic correlations between the dALPS index and 31 phenotypes across 55 genomic loci (Fig. S15b, Table S16). The most significant local genetic associations (FDR <0·05) were observed at locus 17q21·31, chr17: 43,460,501–44,865,832 (Fig. S15c), including AD (local r_g = 0·977), autism spectrum disorder (ASD, local r_g = –1), pulse pressure (PP, local r_g = 0·994), ease of getting up (local r_g = –0·956), daytime napping (local r_g = 1), snoring (local r_g = –1), and post-traumatic stress disorder (PTSD, local r_g = –0·941, Table S17).

Cis-regulated genes/proteins causally associated with the dALPS index

To identify potential genes associated with dALPS, we performed a multi-tissue TWAS using expression profiles from 13 distinct brain subregions and whole blood (Supplementary Methods). Among the 114,674 gene–tissue pairs tested, 340 exhibited (81 genes across 14 tissues) significant associations (FDR <0·05, Fig. 2b, Table S18). We further applied MR-JTI causal inference to these significant gene–tissue pairs and identified 46 gene–tissue pairs with significant causal associations (*P*-values <0·05/340, Bonferroni-corrected threshold, Table S18) spanning 13 brain tissues (Fig. 2b, Table S18). Of the 340 significant gene–tissue pairs, 20 were successfully validated in the independent cohort (Table S18). Moreover, we performed PWAS to investigate the relationship between the dALPS index and protein abundance, and identified 10 proteins associated with dALPS (false discovery rate, FDR <0·05, Fig. 2c, Table S19). Subsequent summary data-based Mendelian randomization (SMR) analysis revealed that six of these proteins—PSMB4, SOD3, RRAS2, SSH2, PYGM, and NSF—exhibited significant causal associations with dALPS index (Fig. 2c, Table S20). Finally, we performed colocalization analysis on all 340 significant gene–tissue pairs from the TWAS and the 10 significant proteins from the PWAS to investigate whether these associations were driven by shared causal variants. This integrated analysis identified five genes (*RP11-798G7·6*, *ARL17B*, *MEN1*, *LRRC37A*, and *C2CD2*; Table S18; Fig. S16a) and two proteins (SOD3, NSF; Table S19, Fig. S16d) that showed strong evidence of colocalization with our dALPS GWAS signal (PP.H4 > 0·8; Tables S18 and S19).

Lifestyle factors associated with the dALPS index

To further investigate the potential environmental and lifestyle determinants of glymphatic function, we examined the associations between the dALPS index and various lifestyles. We revealed that alcohol consumption (particularly wine and champagne), smoking, and sleeping (particularly daytime napping and snoring), were significantly associated with dALPS index (Fig. S18a and b). Specifically, moderate intake of wine and champagne was linked to a slightly higher dALPS index, as

each gene–tissue pair. Gene-tissue pairs with significant causal associations are highlighted with red diamonds. Labels for genes surviving causal analysis are retained only at the most significant locus. The red dashed line represents the significance threshold adjusted for the false discovery rate (FDR <0·05) for two-tailed *P*-values. (**c**) Manhattan plot of PWAS results in brain tissues. Each point represents a protein, with its encoding gene labeled for significant hits. Proteins with significant causal associations are marked with red diamonds. The red dashed line represents the significance threshold adjusted for the false discovery rate (FDR <0·05) for two-tailed *P*-values.

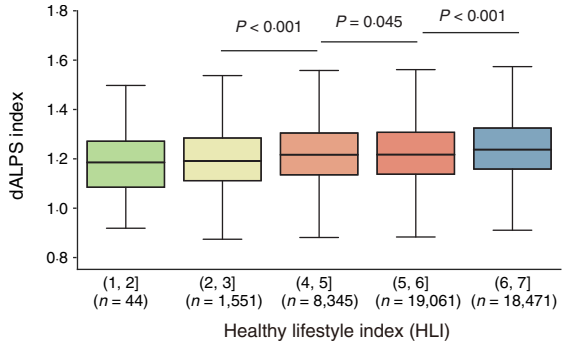

***Fig. 3:* Association between healthy lifestyle index (HLI) and dALPS index.** Box plots represent the distribution of the dALPS index across different categories of the HLI. The upper and lower ends of the boxes represent the IQR (interquartile range) of dALPS index. The lines in the boxes represent the median dALPS index.

consumption levels increased, a negative association emerged (Fig. S18c). We also computed HLI, a composite measure reflecting adherence to health-promoting behaviors, and found a strong positive correlation between dALPS index and higher HLI scores (Fig. 3).

Alterations of dALPS in CNS diseases and the mediating role of medications

We next explored the relationship between dALPS index and various central nervous system (CNS) diseases (Table S22) in UKB. Significant differences in dALPS were observed between disease groups and healthy controls across eight conditions, with all disease groups exhibiting lower dALPS than healthy individuals (Fig. 4a). The most significant reductions were found in multiple sclerosis and depressive episodes (both *P*-value < 0·001), followed by somatoform disorders (P = 0·018) and other anxiety disorders (P = 0·019) (Fig. 4a). Notably, the reduction in dALPS observed in individuals with depression and anxiety disorders was further validated in the EPAD cohort (Fig. 4b). In addition, in disease-specific cohorts, we observed significant correlations between dALPS and established clinical rating scales. For example, in ADNI3 at baseline (AD, Mild Cognitive Impairment [MCI]), higher dALPS was associated with better cognitive performance (Montreal Cognitive Assessment [MoCA], r_s = 0·187; Mini-Mental State Examination [MMSE], r_s = 0·179) and lower dementia rating (Clinical Dementia Rating [CDR], r_s = –0·151), and fewer functional limitations (Functional Activities Questionnaire [FAQ], r_s = –0·195) (Fig. S19a). In PPMI at baseline (PD only), dALPS was inversely correlated with non-motor symptom burden on the rater-completed Movement Disorder Society–Unified Parkinson's Disease Rating Scale (MDS-UPDRS) Part I total score (Non-Motor Aspects of Experiences of Daily Living total score [NP1RTOT], r_s = –0·152) (Fig. S19b). These results further support the clinical relevance of dALPS as a biomarker linked to cognitive impairment and disease severity.

We also performed a mediation analysis to assess whether drug usage (Table S23) mediates the relationship between depression or anxiety disorders and dALPS. We observed that drug use played a significant mediating role in the relationship between depression and dALPS (P = 0·020) (Fig. 4c), but no mediation effect in the context of other anxiety disorders (P = 0·66) (Fig. 4d), and these findings were validated in the EPAD cohort (Fig. S20a–c). To explore whether specific classes of antidepressants contributed differentially to this mediation effect, we stratified the 58 antidepressants into ten mechanistically defined categories (Table S24). Among these, four drug classes—SSRIs, TCAs, SNRIs, and NaSSAs—had sufficient sample sizes (n > 100) for subgroup mediation analyses. We found that SSRIs and TCAs exhibited significant mediating effects, accounting for 21·1% and 10·5% of the mediation percentage of depression on dALPS, respectively (Fig. S21a and b, Table S25). In contrast, no significant mediation effects were observed for SNRIs and NaSSAs (Fig. S21c and d, Table S25). Notably, the mediating role of SSRIs was independently confirmed in the EPAD cohort (Fig. S20b, Table S25).

Since sleep medications have been found to disrupt the brain's waste clearance during sleep,[38] we analyzed whether disease or insomnia affected dALPS through the use of sleep medications, primarily benzodiazepines and Z-drugs. We did not observe the use of sleep medications mediate the relationship between either disease or insomnia and dALPS (Fig. S22a and b, Table S26). Although diseases and insomnia can influence medication use, the effect of medication on dALPS index was not significant (Fig. S22a and b, Table S26). This suggests that the impact of sleep medications on dALPS was not substantial, and their usage did not significantly alter dALPS index in these cases.

Furthermore, we examined whether baseline dALPS index was associated with the future risk of CNS diseases. Cox regression analysis revealed that lower baseline dALPS index was associated with an increased risk of developing AD, cerebrovascular diseases, and hydrocephalus, with the strongest association observed for AD (Fig. 4e). This relationship remained significant after adjusting for age, sex, and *APOE* ε4 status (Fig. S23a), and was validated in the OASIS3 cohort (Fig. S23b).

Discussion

In this study, we developed a deep learning-based automation of the DTI-ALPS procedure, which should be understood as a diffusion-derived proxy sensitive to water motion along perivascular spaces rather than a direct measurement of glymphatic flux. This framing

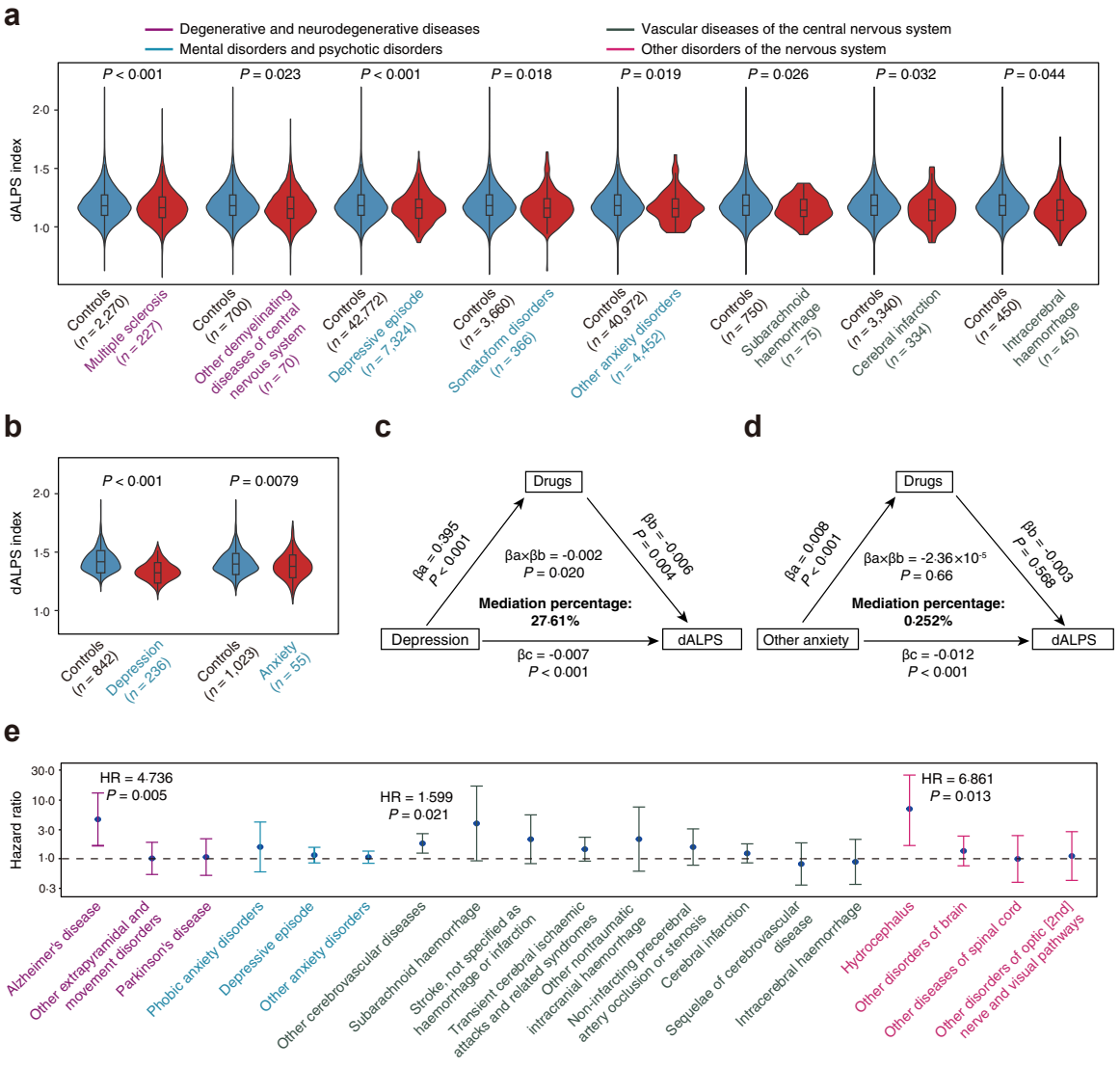

Fig. 4: **Association between dALPS and CNS diseases.** (**a**) Eight different CNS disease groups showed significantly lower dALPS index compared to healthy individuals. (**b**) Violin plots illustrating significantly reduced dALPS index in patients with depression and anxiety disorders compared to healthy controls in the European Prevention of Alzheimer's Dementia (EPAD) study. Mediation analysis evaluated whether drug use might explain the link between depression (**c**) and anxiety disorder (**d**) and dALPS reduction. (**e**) Cox regression analysis was performed to examine whether baseline dALPS index could predict the future risk of developing CNS diseases. HR, hazard ratio.

follows recent reviews that revisit both the rationale and the interpretational caveats of DTI-ALPS. [39] We adopted a lightweight VGG backbone for CNN slice classification and YOLOv5s for ROI detection because the recognition tasks were straightforward and the anatomical features were highly distinctive. Compared to more complex networks (e.g., ResNet, Mask R-CNN), the simpler architectures converged rapidly and avoided unnecessary overfitting while still achieving excellent performance (AUC = 0·989 for CNN, mAP@0·5 = 0·993 for YOLOv5). Therefore, minimal augmentation and default hyperparameter settings were sufficient. By leveraging CNN and YOLOv5-based ROI detection, we achieved highly accurate and automated identification of ALPS-related ROIs, overcoming key limitations of manual ROI placing. Through large-scale analysis of over 65,000 individuals, we revealed that dALPS shows sex- and age-related differences and is linked to several body composition and cardiovascular traits. Furthermore, our GWAS identified five genetic loci linked to dALPS, highlighting a substantial genetic contribution to glymphatic function. Multi-omics integration via TWAS, PWAS, and colocalization uncovered potential causal genes and proteins, providing novel insights into

the molecular pathways governing brain fluid dynamics. Additionally, we identified a strong positive association between the dALPS index and the HLI, suggesting that adherence to healthier lifestyle behaviors is linked to improved glymphatic function. Furthermore, dALPS was significantly correlated with clinical rating scales across independent cohorts: in ADNI3 (AD, MCI) with cognition (MoCA/MMSE) and dementia rating (CDR), and in PPMI (PD) with non-motor symptoms (NP1RTOT). A PD-focused meta-analysis found that the DTI-ALPS index was significantly associated with MDS-UPDRS III and Hoehn–Yahr stage.[40] In AD, a recent systematic review reported that DTI-ALPS was reduced in AD and MCI versus controls and correlates with global cognition (e.g., MMSE)[41]—consistent with our ADNI3 findings. These results support the clinical relevance of dALPS as a biomarker linked to both cognitive decline and functional impairment in neurodegenerative diseases. Importantly, we showed that reduced dALPS index is associated with multiple CNS disorders, including depression, anxiety and neurodegenerative diseases, with lower baseline dALPS predicting higher future risk of AD and cerebrovascular conditions. Thus, we suggest that dALPS is a powerful imaging-derived biomarker with broad implications for studying brain waste clearance, neurological health and disease susceptibility.

Automated, large-scale calculation of DTI-ALPS typically involves normalizing individual DTI data to a standardized anatomical space using image registration methods. For instance, Huang et al. utilized a group-averaged ROI template to facilitate DTI-ALPS measurements across extensive cohorts,[22] whereas Ran et al. employed the widely-adopted ANTsX spatial normalization tool to register individual FA images to the FA template provided by the JHU DTI atlas,[21] which is the most commonly employed strategy for calculating DTI-ALPS index in neuroimaging studies. However, it should be noted that such template-based registration approaches may suffer from reduced accuracy in brains exhibiting significant anatomical atrophy—a common phenomenon in elderly populations.[42] Brain atrophy often leads to structural deformation,[43] which causes misalignment between standardized templates and individual FA images,[44] thereby compromising the precision of the derived DTI-ALPS index. The conventional procedure for calculating the DTI-ALPS index is relatively straightforward, primarily involving the selection of a slice at the body of the lateral ventricles from axial brain images, followed by placing ROIs on each side of this slice (in some cases, ROIs on the left and right sides may not be drawn on the same slice), and then computing the DTI-ALPS index using the established formula.[11] Our dALPS approach automated the aforementioned process, being able to measure the DTI-ALPS index in large-scale cohorts and investigate the genetic and molecular mechanisms underlying the glymphatic function. In doing so, our pipeline formalizes the geometric rationale of the original DTI-ALPS method—ventricular-body slice selection and ROI placement along projection and association fibers—while removing operator dependence via CNN-based slice selection and YOLOv5 ROI detection. Consistent with the reproducibility findings of Taoka et al.,[45] we therefore treat manual DTI-ALPS as an expert reference rather than a physiological gold standard, and evaluate dALPS against this reference using agreement-focused metrics (ICC, CCC, Bland–Altman). Furthermore, in line with the review by Taoka et al.,[39] our contribution should be interpreted as automating expert best-practice ROI selection and scaling it to population studies, while acknowledging the interpretational limitations inherent to DTI-ALPS. To enhance the generalizability of our tool and improve its adaptability to diverse populations, we selected DTI images from 500 Chinese individuals and 500 European Caucasians to construct our models. The CNN model achieved a validation set AUC of 0·989 and PRC of 0·883, demonstrating robust multi-slice identification around the lateral ventricle regions. The YOLOv5 model exhibited strong training convergence with a high mAP of 0·993, reflecting precise and reliable target localization. Our dALPS workflow showed excellent agreement with traditional manual approaches (ICC = 0·95), underscoring its reliability and practical utility. At the same time, the correlation between the two methods remained moderate (r = 0·55), suggesting the presence of numerical differences. This discrepancy may stem from the increased sensitivity of the deep learning-based DTI-ALPS method, which likely captures subtle variations that manual methods might overlook. Additionally, manual approaches inherently involve subjective judgment, whereas the automated dALPS analysis minimizes such biases. Notably, the capability of dALPS to automatically identify multiple slices offers a more comprehensive analysis compared to traditional single-slice selection, potentially contributing to the observed numerical differences. Overall, our dALPS minimizes dependence on operator expertise, thereby improving objectivity, reproducibility and the overall consistency of DTI-ALPS index measurement. As emphasized by Taoka et al.,[39,45] manual DTI-ALPS should be regarded as an expert-derived reference rather than a physiological gold standard, and numerical differences between automated and manual approaches should be interpreted as method-level variation within the broader limitations of the DTI-ALPS framework.

In contrast to the previous studies,[21,22] we performed the largest GWAS of DTI-ALPS to date, with a total sample size of 53,719. Among the 34 SNPs significantly associated with the mean dALPS index, four of them were also identified as significant (P-value < 5×10^{-8}) in the recent GWAS of the mean DTI-ALPS index

performed by Huang et al., including the most significant variant, rs12146713 (Table S13).[22] However, no overlapping significant SNPs (P-value < 5×10^{-8}) were found in the study by Ran et al. (Table S13),[21] which may be attributed to differences in DTI-ALPS index calculation methods and sample sizes across studies. The most significant locus we identified, rs12146713, has been previously reported to be associated with accelerated brain ageing,[46] which is analogous with our observation that mutations are linked to a decline in the dALPS index. Notably, rs12146713 is located in *NUAK1*, which mediates Ser356 phosphorylation of tau. This phosphorylation destabilizes microtubules, promotes tau release, and impedes proteasomal degradation of tau, thereby exacerbating tau hyperphosphorylation and aggregation. These pathological mechanisms are hallmarks of AD neuropathology,[47] but the roles of *NUAK1* in glymphatic system remained unclear. The glymphatic system has been implicated in various central nervous system disorders and sleep disturbances,[48] and our genetic correlation analyses provide further support for these associations. We discovered that the dALPS index shares a common genetic architecture with neurological disorders, brain structures, and sleep-related traits. Notably, the genomic region 17q21·31 exhibits the highest number of local genetic correlations. This region contains genes such as *MAPT*, *MAPT-AS1*, *KANSL1*, and *LRRC37A*, among others (Fig. S15c), which have been strongly linked to various neurological disorders.[49] Whether this shared genetic mechanism promotes or mitigates the related symptoms requires further investigation. We further performed TWAS and PWAS and identified potential causal effects genes on dALPS index. *LRRC37A*, *CABYR*, and *MAPT-AS1* are among the top TWAS protein coding gene associations identified through causal analysis. In the colocalization analysis, *LRRC37A* emerged as a particularly compelling candidate, as its lead *cis*-eQTL corresponded to one of the primary lead GWAS SNPs (rs7225002, Fig. S14d). Furthermore, we found *LRRC37A* was consistent associations with the trait in the initial TWAS across multiple brain regions (Table S18), supporting its role as a likely mediator of the GWAS signal. Notably, *LRRC37A* showed the strongest overall association with the dALPS index, with significant associations across 13 tissues (Fig. 2b, Table S18). Previous studies have established *LRRC37A* as a TWAS significant gene linked to brain structure.[50] Moreover, postmortem RNAseq based eQTL analyses have shown that *LRRC37A* expression is associated with the caudal middle frontal thickness.[51] *CABYR*, primarily expressed in the testes and involved in sperm capacitation, has been reported to exhibit higher expression in fetal brains compared to adult brains, suggesting a potential role in brain development.[52] *MAPT-AS1* is a natural antisense transcript (NAT) closely associated with the *MAPT*, which encodes the microtubule-associated protein tau. In our TWAS, *MAPT-AS1* exhibited significant associations across nine tissues and was identified as a causal gene in four tissues: the amygdala, cerebellum, hypothalamus, and spinal cord (cervical c-1). Previous studies have reported that *MAPT-AS1* inhibits tau protein translation and shows a negative correlation with tau pathology (Braak staging) in the brain.[53] Additionally, several long non-coding RNAs (lncRNAs) were identified through causal analysis (Fig. 2b, Table S18), although numerous studies have established that lncRNAs play critical roles in neurodevelopment and neurodegenerative diseases, limited research has linked the lncRNAs identified in this study to brain structure, function, and diseases.[54] We identified three genes/proteins—*PSMB4*, *PYGM*, and *SOD3*—as causal candidates, as they were consistently implicated in both TWAS and PWAS (Fig. 2b–c). *PSMB4*, a component of the multicatalytic proteasome complex, plays a crucial role in ATP/ubiquitin-dependent protein degradation and maintaining intracellular proteostasis. Integrative analysis of GWAS and human plasma proteomics has identified *PSMB4* as a potential biomarker and therapeutic target for depression.[55] Additionally, in a lipopolysaccharide (LPS)-induced neuroinflammatory rat model, *PSMB4* expression was significantly elevated in apoptotic neurons, suggesting its potential involvement in neurodegenerative diseases.[56] *PYGM* encodes myophosphorylase, an enzyme that catalyzes glycogenolysis. While previous studies have primarily associated *PYGM* with glycogen storage diseases.[57] and a recent study revealed that neuronal downregulation of *PYGM* in wild-type mice impaired synaptic plasticity and cognitive function, while its overexpression in AD mice ameliorated synaptic dysfunction and cognitive deficits.[58] *SOD3* encodes extracellular superoxide dismutase, an enzyme that catalyzes the conversion of superoxide radicals into hydrogen peroxide and oxygen, thereby protecting cells from oxidative stress damage.[59] Previous studies have demonstrated that *SOD3* plays a pivotal role in cerebral vascular and vasomotor function, while also providing neuroprotective effects.[60] Finally, to further elucidate the functional context of the genetic variants associated with the dALPS index, we integrated our results with a multi-region single-nucleus RNA-seq dataset derived from postmortem brain samples. This analysis revealed a significant enrichment in vascular cells, particularly within the globus pallidus interna (GPI), primary motor cortex (PMC), dorsolateral prefrontal cortex (DLPFC, Table S21, Fig. S17e). These findings are especially relevant given that the glymphatic system is intrinsically coupled to the brain's vascular network.

Previous studies have reported that the DTI-ALPS index decreases with advancing age, exhibits higher values in females compared to males, and is notably associated with obesity-related traits and pulse rate.[21,22]

A recent study in patients with PD further confirmed a significant negative correlation between BMI and the DTI-ALPS index, with obese patients exhibiting significantly reduced glymphatic function compared to normal-weight individuals.[61] Our deep learning-based dALPS index showed consistent trends, aligning closely with these prior observations, and this consistency underscores the reproducibility and reliability of the dALPS approach. The robustness of associations between the dALPS index and demographic characteristics highlights the stability of this phenomenon across different measurement methodologies. These findings further support the validity of the dALPS index as a promising biomarker for assessing glymphatic function in the brain. Additionally, the association with obesity-related traits suggests that elevated BMI might impair glymphatic clearance, potentially increasing the risk of neurodegenerative conditions and highlighting the clinical importance of managing obesity to maintain optimal brain health. HLI reflects a composite measure encompassing multiple beneficial behaviors, including a balanced diet, regular physical activity, adequate sleep, moderate alcohol consumption, and non-smoking status.[62] Our study observed higher dALPS among subjects with elevated HLI scores, suggesting a potential protective effect of maintaining a healthy lifestyle on glymphatic system functionality. Further research is warranted to investigate whether targeted interventions aimed at improving lifestyle factors could effectively enhance dALPS and, consequently, bolster glymphatic function in the brain.

More evidence suggests that DTI-ALPS is reduced across various neurological disorders, including multiple sclerosis,[63] depression,[64] and intracerebral hemorrhage.[65] Our findings support the previous observations and additionally provide evidence linking the DTI-ALPS index with anxiety, somatoform disorder, subarachnoid hemorrhage, and cerebral infarction. These findings underscore the potential of the dALPS index as a valuable biomarker for assessing the impact of multiple CNS disorders. The associations with anxiety and somatoform disorder are particularly noteworthy, as both conditions have traditionally been considered psychological disorders. Their connections to glymphatic function suggest possible underlying biological mechanisms. Future research may explore whether interventions aimed at improving glymphatic clearance (e.g., enhancing sleep quality, reducing inflammation or optimizing vascular function) could help alleviate the pathological impacts associated with these mental health disorders. Notably, our mediation analyses suggest that drug usage for depression could impact the glymphatic system, consequently reducing the dALPS index. This may partly explain the impaired glymphatic function observed in depressed patients, beyond the direct effects of depression itself. It is important to clarify that our mediation analysis was not designed as a pharmacological study of antidepressant effects per se, but as a statistical exploration of whether medication use might account for part of the observed association between psychiatric diagnosis and reduced dALPS. Nevertheless, since our primary model treated psychiatric diagnosis as the independent variable and drug usage as the mediator, these unmeasured treatment parameters are conceptually downstream of the mediator itself and would not invalidate the interpretability of the indirect pathway. Consequently, our findings should be understood as revealing a statistical mediation pattern—suggesting that antidepressant use may partially explain the observed link between depression and reduced dALPS—rather than demonstrating a direct causal pharmacological effect. In the UKB cohort, the four most commonly used classes of antidepressants were SSRIs, TCAs, SNRIs, and NaSSAs. We found that SSRIs and TCAs had significant mediating effects, accounting for 21·1% and 10·5% of the association between depression and reduced dALPS, respectively. While SSRIs primarily function by elevating serotonin levels,[66] emerging evidence suggests that they may still influence CSF circulation, blood–brain barrier (BBB) permeability, and neuroinflammatory pathways[67,68]—all of which are tightly linked to CSF dynamics and glymphatic function. TCAs exhibit broader actions, affecting both serotonin and norepinephrine systems and possessing significant anticholinergic properties, potentially exerting more complex effects on cerebral blood flow and metabolism.[69] Consequently, both SSRIs and TCAs might alter sleep architecture and cerebral metabolism, leading to changes in nocturnal glymphatic efficiency. In contrast, no significant mediation effects were observed for SNRIs and NaSSAs, despite their modulation of multiple neurotransmitter systems.[70] This could be due to smaller sample sizes limiting the statistical power to detect glymphatic alterations, and it is also possible that the pharmacological mechanisms of these drugs exert relatively weak effects on the glymphatic system. Given these differential impacts of various antidepressants on brain clearance function, the therapeutic strategies for depression should explicitly account for these potential neurometabolic side effects. Traditionally, evaluations of antidepressant side effects have predominantly emphasized cognitive, emotional, or systemic parameters, such as changes in body weight or gastrointestinal function.[71,72] Our findings underscore the importance of incorporating 'brain clearance function' as an additional dimension in assessing drug impacts, particularly in populations undergoing chronic pharmacological treatment.

Our study has several limitations. Firstly, the analysis primarily utilized data from the UKB, predominantly composed of individuals of European ancestry, with limited representation of non-European populations. Although we included DTI data from 500 Chinese participants during model training to enhance

generalizability, further validation in more diverse and multi-ethnic cohorts is essential to confirm the stability and reproducibility of the dALPS method across different populations. Secondly, despite employing CNN and YOLOv5 models for automated ROI detection, significantly reducing human error, DTI itself remains susceptible to inherent limitations associated with MRI scanning, such as resolution constraints and noise. Subtle motion artifacts or magnetic field inhomogeneities, for instance, may affect the accuracy of FA calculations, thereby influencing the reliability of the ALPS index. Moreover, although our findings reveal significant associations between dALPS and various factors such as age, sex, lifestyle, genetic variants, and multiple CNS disorders, the precise physiological and pathological interpretations remain to be fully elucidated. Another limitation is that we were unable to verify whether the observed lower dALPS index in the disease group, compared to healthy controls, reflects a causal relationship. The dALPS index primarily reflects directional water diffusion within the brain, and whether it directly corresponds to glymphatic function remains a matter of debate and should be interpreted cautiously.[39,45] Future research integrating dynamic contrast-enhanced MRI (DCE-MRI) or in vivo tracer experiments could provide more direct evidence to validate the relationship between dALPS and cerebrospinal fluid dynamics, enhancing the biological relevance and interpretability of this imaging biomarker. Additionally, given the findings from our mediation analysis, future investigations employing animal models or human functional neuroimaging are essential, which could more definitively establish whether antidepressants directly influence glymphatic clearance efficiency via modulation of BBB integrity, cerebral blood flow, or sleep architecture. More importantly, whether and how to optimize antidepressant regimens requires more well-designed clinical studies.

Contributors

C.L. and H.W. contributed equally to this work. C.L. and G.L. conceived and designed the study. C.L., H.W., W.X., Y.Z., W.D., X.C., J.L., W.C., L.L., F.S., Z.P., and G.L. contributed to data acquisition, analysis, and interpretation. C.L. and H.W. drafted the manuscript. Z.P. and G.L. critically revised the manuscript for important intellectual content. Statistical analyses were performed by C.L., H.W., W.D., X.C., J.L., W.C., and L.L. Funding was obtained by Z.P. and G.L. Administrative, technical, and material support were provided by Z.P. and G.L. G.L. and C.L. had full access to all data in the study and take responsibility for the integrity of the data and the accuracy of the analysis. All authors read, reviewed and approved the final manuscript. The ADNI and EPAD Consortia contributed by establishing and maintaining the study cohorts, generating and curating the datasets used in this study, and overseeing data access and use.

Data sharing statement

The clinical and neuroimaging data for PPMI and ADNI are publicly available upon request at ppmi@loni.usc.edu and https://adni.loni.usc.edu. Requests for access to the neuroimaging data for GHAD (Guangzhou Healthy Aging and Dementia Cohort) and GPMP (Guangzhou Precision Medicine Parkinson's Cohort) can be directed to peizhong@mail.sysu.edu.cn, including the proposed purpose for data use, and are subject to governance constraints and privacy restrictions. The dALPS pipeline code is available at https://github.com/sixguns1984/dALPS. The GWAS summary statistics for the dALPS index are publicly available at https://doi.org/10.6084/m9.figshare.30937796.

Declaration of interests

The authors declare that they have no competing interests.

Acknowledgements

We thank all study participants and their families, investigators, and members of PPMI, ADNI, GHAD, GPMP, UKB, OASIS, EPAD and AMP-PD. We conducted this research under the UK Biobank application no. 109145. This study is supported by High-performance Computing Public Platform (Shenzhen Campus) of Sun Yat-sen University.

ADNI: Data collection and sharing for this project was funded by the Alzheimer's Disease Neuroimaging Initiative (ADNI) (National Institutes of Health Grant U01 AG024904) and DOD ADNI (Department of Defense award number W81XWH-12-2-0012). ADNI is funded by the National Institute on Aging, the National Institute of Biomedical Imaging and Bioengineering, and through generous contributions from the following: AbbVie, Alzheimer's Association; Alzheimer's Drug Discovery Foundation; Araclon Biotech; BioClinica, Inc.; Biogen; Bristol-Myers Squibb Company; CereSpir, Inc.; Cogstate; Eisai Inc.; Elan Pharmaceuticals, Inc.; Eli Lilly and Company; EuroImmun; F. Hoffmann-La Roche Ltd and its affiliated company Genentech, Inc.; Fujirebio; GE Healthcare; IXICO Ltd.; Janssen Alzheimer Immunotherapy Research & Development, LLC.; Johnson & Johnson Pharmaceutical Research & Development LLC.; Lumosity; Lundbeck; Merck & Co., Inc.; Meso Scale Diagnostics, LLC.; NeuroRx Research; Neurotrack Technologies; Novartis Pharmaceuticals Corporation; Pfizer Inc.; Piramal Imaging; Servier; Takeda Pharmaceutical Company; and Transition Therapeutics. The Canadian Institutes of Health Research is providing funds to support ADNI clinical sites in Canada. Private sector contributions are facilitated by the Foundation for the National Institutes of Health (www.fnih.org). The grantee organization is the Northern California Institute for Research and Education, and the study is coordinated by the Alzheimer's Therapeutic Research Institute at the University of Southern California. ADNI data are disseminated by the Laboratory for Neuro Imaging at the University of Southern California.

Data used in preparation of this article were obtained from the Alzheimer's Disease Neuroimaging Initiative (ADNI) database (adni.loni.usc.edu). As such, the investigators within the ADNI contributed to the design and implementation of ADNI and/or provided data but did not participate in analysis or writing of this report. A complete listing of ADNI investigators can be found at http://adni.loni.usc.edu/wp-content/uploads/how_to_apply/ADNI_Acknowledgement_List.pdf.

PPMI: Data used in the preparation of this article were obtained [on November, 14 2022] from the Parkinson's Progression Markers Initiative (PPMI) database (www.ppmi-info.org/access-dataspecimens/download-data), RRID: SCR 006431. This analysis used MRI imaging data for PD participants, obtained from PPMI upon request after approval by the PPMI Data Access Committee. For up-to-date information on the study, visit www.ppmi-info.org. PPMI – a public-private partnership – is funded by the Michael J. Fox Foundation for Parkinson's Research and funding partners, including 4D Pharma, AbbVie, AcureX, Allergan, Amathus Therapeutics, Aligning Science Across Parkinson's, AskBio, Avid Radiopharmaceuticals, BIAL, Biogen, Biohaven, BioLegend, BlueRock Therapeutics, Bristol-Myers Squibb, Calico Labs, Celgene, Cerevel Therapeutics, Coave Therapeutics, DaCapo Brainscience, Denali, Edmond J. Safra Foundation, Eli Lilly, Gain Therapeutics, GE HealthCare, Genentech, GSK, Golub Capital, Handl Therapeutics, Insitro, Janssen Neuroscience, Lundbeck, Merck, Meso Scale Discovery, Mission Therapeutics, Neurocrine Biosciences, Pfizer, Piramal, Prevail Therapeutics, Roche, Sanofi, Servier, Sun Pharma Advanced Research Company, Takeda, Teva, UCB, Vanqua Bio, Verily,

Voyager Therapeutics, the Weston Family Foundation and Yumanity Therapeutics.

EPAD: EPAD LCS is registered at www.clinicaltrials.gov Identifier: NCT02804789. Data used in preparation of this article were obtained from the EPAD LCS data set Version.IMI (V.IMI), doi: 10.34688/epadlcs_v.imi_20.10.30. The EPAD LCS was launched in 2015 as a public private partnership, led by Chief Investigator Professor Craig Ritchie MB BS. The primary research goal of the EPAD LCS is to provide a well-phenotyped probability-spectrum population for developing and continuously improving disease models for Alzheimer's disease in individuals without dementia. This work used data and/or samples from the EPAD project which received support from the EU/EFPIA Innovative Medicines Initiative Joint Undertaking EPAD grant agreement no. 115736 and an Alzheimer's Association Grant (SG21-818099-EPAD).

Data used in preparation of this article were obtained from the Longitudinal Cohort Study (LCS), delivered by the European Prevention of Alzheimer's Disease (EPAD) Consortium. As such investigators within the EPAD LCS and EPAD Consortium contributed to the design and implementation of EPAD and/or provided data but did not participate in analysis or writing of this report. A complete list of EPAD Investigators can be found at: http://ep-ad.org/wp-content/uploads/2020/12/202010_List-of-epadistas.pdf.

The snRNA-seq data (the release 4·0 post-mortem sequencing cohort) used in the preparation of this article were obtained from the Accelerating Medicine Partnership® (AMP®) Parkinson's Disease (AMP PD) Knowledge Platform. For up-to-date information on the study, visit https://www.amp-pd.org.

The AMP® PD program is a public-private partnership managed by the Foundation for the National Institutes of Health and funded by the National Institute of Neurological Disorders and Stroke (NINDS) in partnership with the Aligning Science Across Parkinson's (ASAP) initiative; Celgene Corporation, a subsidiary of Bristol-Myers Squibb Company; GlaxoSmithKline plc (GSK); The Michael J. Fox Foundation for Parkinson's Research; Pfizer Inc.; AbbVie Inc.; Sanofi US Services Inc.; and Verily Life Sciences.

ACCELERATING MEDICINES PARTNERSHIP and AMP are registered service marks of the U.S. Department of Health and Human Services.

Appendix A. Supplementary data

Supplementary data related to this article can be found at https://doi.org/10.1016/j.ebiom.2026.106133.

References

1 Iliff JJ, Wang M, Liao Y, et al. A paravascular pathway facilitates CSF flow through the brain parenchyma and the clearance of interstitial solutes, including amyloid β. *Sci Transl Med*. 2012;4(147):147ra111. https://doi.org/10.1126/scitranslmed.3003748.
2 Hardy J, Selkoe DJ. The amyloid hypothesis of Alzheimer's disease: progress and problems on the road to therapeutics. *Science*. 2002;297(5580):353–356. https://doi.org/10.1126/science.1072994.
3 Dickson DW. Neuropathology of Parkinson disease. *Parkinsonism Relat Disord*. 2018;46 Suppl 1(Suppl 1):S30–s33. https://doi.org/10.1016/j.parkreldis.2017.07.033.
4 Iliff JJ, Lee H, Yu M, et al. Brain-wide pathway for waste clearance captured by contrast-enhanced MRI. *J Clin Invest*. 2013;123(3):1299–1309. https://doi.org/10.1172/jci67677.
5 Taoka T, Naganawa S. Glymphatic imaging using MRI. *J Magn Reson Imaging*. 2020;51(1):11–24. https://doi.org/10.1002/jmri.26892.
6 Keil SA, Braun M, O'Boyle R, et al. Dynamic infrared imaging of cerebrospinal fluid tracer influx into the brain. *Neurophotonics*. 2022;9(3):031915. https://doi.org/10.1117/1.NPh.9.3.031915.
7 Han F, Chen J, Belkin-Rosen A, et al. Reduced coupling between cerebrospinal fluid flow and global brain activity is linked to Alzheimer disease-related pathology. *PLoS Biol*. 2021;19(6):e3001233. https://doi.org/10.1371/journal.pbio.3001233.
8 Harrison IF, Siow B, Akilo AB, et al. Non-invasive imaging of CSF-mediated brain clearance pathways via assessment of perivascular fluid movement with diffusion tensor MRI. *Elife*. 2018;7:e34028. https://doi.org/10.7554/eLife.34028.
9 Han G, Zhou Y, Zhang K, et al. Age- and time-of-day dependence of glymphatic function in the human brain measured via two diffusion MRI methods. *Front Aging Neurosci*. 2023;15:1173221. https://doi.org/10.3389/fnagi.2023.1173221.
10 Ringstad G, Vatnehol SAS, Eide PK. Glymphatic MRI in idiopathic normal pressure hydrocephalus. *Brain*. 2017;140(10):2691–2705. https://doi.org/10.1093/brain/awx191.
11 Taoka T, Masutani Y, Kawai H, et al. Evaluation of glymphatic system activity with the diffusion MR technique: diffusion tensor image analysis along the perivascular space (DTI-ALPS) in Alzheimer's disease cases. *Jpn J Radiol*. 2017;35(4):172–178. https://doi.org/10.1007/s11604-017-0617-z.
12 Qin Y, He R, Chen J, et al. Neuroimaging uncovers distinct relationships of glymphatic dysfunction and motor symptoms in Parkinson's disease. *J Neurol*. 2023;270(5):2649–2658. https://doi.org/10.1007/s00415-023-11594-5.
13 Si X, Guo T, Wang Z, et al. Neuroimaging evidence of glymphatic system dysfunction in possible REM sleep behavior disorder and Parkinson's disease. *NPJ Parkinsons Dis*. 2022;8(1):54. https://doi.org/10.1038/s41531-022-00316-9.
14 Xie Y, Zhu H, Yao Y, et al. Enlarged choroid plexus in relapsing-remitting multiple sclerosis may lead to brain structural changes through the glymphatic impairment. *Mult Scler Relat Disord*. 2024;85:105550. https://doi.org/10.1016/j.msard.2024.105550.
15 Qin Y, Li X, Qiao Y, et al. DTI-ALPS: an MR biomarker for motor dysfunction in patients with subacute ischemic stroke. *Front Neurosci*. 2023;17:1132393. https://doi.org/10.3389/fnins.2023.1132393.
16 Zhu H, Xie Y, Li L, et al. Diffusion along the perivascular space as a potential biomarker for glioma grading and isocitrate dehydrogenase 1 mutation status prediction. *Quant Imaging Med Surg*. 2023;13(12):8259–8273. https://doi.org/10.21037/qims-23-541.
17 Tu Y, Li Z, Xiong F, Gao F. Decreased DTI-ALPS and choroid plexus enlargement in fibromyalgia: a preliminary multimodal MRI study. *Neuroradiology*. 2023;65(12):1749–1755. https://doi.org/10.1007/s00234-023-03240-8.
18 Saito Y, Kamagata K, Uchida W, Takabayashi K, Aoki S. Improved reproducibility of diffusion tensor image analysis along the perivascular space (DTI-ALPS) index calculated by manual and automated methods. *Jpn J Radiol*. 2023;41(9):1033–1034. https://doi.org/10.1007/s11604-023-01429-8.
19 Tatekawa H, Matsushita S, Ueda D, et al. Improved reproducibility of diffusion tensor image analysis along the perivascular space (DTI-ALPS) index: an analysis of reorientation technique of the OASIS-3 dataset. *Jpn J Radiol*. 2023;41(4):393–400. https://doi.org/10.1007/s11604-022-01370-2.
20 Liu X, Barisano G, Shao X, et al. Cross-Vendor test-retest validation of diffusion tensor image analysis along the perivascular space (DTI-ALPS) for evaluating glymphatic system function. *Aging Dis*. 2024;15:1885–1898. https://doi.org/10.14336/ad.2023.0321-2.
21 Ran L, Fang Y, Cheng C, et al. Genome-wide and phenome-wide studies provided insights into brain glymphatic system function and its clinical associations. *Sci Adv*. 2025;11(3):eadr4606. https://doi.org/10.1126/sciadv.adr4606.
22 Huang SY, Ge YJ, Ren P, et al. Genome-wide association study unravels mechanisms of brain glymphatic activity. *Nat Commun*. 2025;16(1):626. https://doi.org/10.1038/s41467-024-55706-9.
23 Bycroft C, Freeman C, Petkova D, et al. The UK Biobank resource with deep phenotyping and genomic data. *Nature*. 2018;562(7726):203–209. https://doi.org/10.1038/s41586-018-0579-z.
24 Chang CC, Chow CC, Tellier LC, Vattikuti S, Purcell SM, Lee JJ. Second-generation PLINK: rising to the challenge of larger and richer datasets. *Gigascience*. 2015;4(7):7. https://doi.org/10.1186/s13742-015-0047-8.
25 Jiang L, Zheng Z, Qi T, et al. A resource-efficient tool for mixed model association analysis of large-scale data. *Nat Genet*. 2019;51(12):1749–1755. https://doi.org/10.1038/s41588-019-0530-8.
26 Yang J, Lee SH, Goddard ME, Visscher PM. GCTA: a tool for genome-wide complex trait analysis. *Am J Hum Genet*. 2011;88(1):76–82. https://doi.org/10.1016/j.ajhg.2010.11.011.
27 Yang J, Ferreira T, Morris AP, et al. Conditional and joint multiple-SNP analysis of GWAS summary statistics identifies additional variants influencing complex traits. *Nat Genet*. 2012;44(4):369–375. S1-S3 https://doi.org/10.1038/ng.2213.

28 Bulik-Sullivan BK, Loh PR, Finucane HK, et al. LD score regression distinguishes confounding from polygenicity in genome-wide association studies. *Nat Genet*. 2015;47(3):291–295. https://doi.org/10.1038/ng.3211.

29 Gamazon ER, Wheeler HE, Shah KP, et al. A gene-based association method for mapping traits using reference transcriptome data. *Nat Genet*. 2015;47(9):1091–1098. https://doi.org/10.1038/ng.3367.

30 Zhou D, Jiang Y, Zhong X, Cox NJ, Liu C, Gamazon ER. A unified framework for joint-tissue transcriptome-wide association and Mendelian randomization analysis. *Nat Genet*. 2020;52(11): 1239–1246. https://doi.org/10.1038/s41588-020-0706-2.

31 Gusev A, Ko A, Shi H, et al. Integrative approaches for large-scale transcriptome-wide association studies. *Nat Genet*. 2016;48(3): 245–252. https://doi.org/10.1038/ng.3506.

32 Wingo TS, Liu Y, Gerasimov ES, et al. Shared mechanisms across the major psychiatric and neurodegenerative diseases. *Nat Commun*. 2022;13(1):4314. https://doi.org/10.1038/s41467-022-31873-5.

33 Zhu Z, Zhang F, Hu H, et al. Integration of summary data from GWAS and eQTL studies predicts complex trait gene targets. *Nat Genet*. 2016;48(5):481–487. https://doi.org/10.1038/ng.3538.

34 Wallace C. Eliciting priors and relaxing the single causal variant assumption in colocalisation analyses. *PLoS Genet*. 2020;16(4): e1008720. https://doi.org/10.1371/journal.pgen.1008720.

35 Zhang MJ, Hou K, Dey KK, et al. Polygenic enrichment distinguishes disease associations of individual cells in single-cell RNA-seq data. *Nat Genet*. 2022;54(10):1572–1580. https://doi.org/10.1038/s41588-022-01167-z.

36 Wang J, Du W, Chen X, Wu H, Liu G. Hypoxia and TTR dysregulation in astrocytes from Parkinson's disease with a specific mitochondrial haplogroup: a single-cell analysis. *Neural Regen Res*. 2025. https://doi.org/10.4103/nrr.Nrr-d-25-00107.

37 Yang J, Benyamin B, McEvoy BP, et al. Common SNPs explain a large proportion of the heritability for human height. *Nat Genet*. 2010;42(7):565–569. https://doi.org/10.1038/ng.608.

38 Hauglund NL, Andersen M, Tokarska K, et al. Norepinephrine-mediated slow vasomotion drives glymphatic clearance during sleep. *Cell*. 2025;188(3):606–622.e17. https://doi.org/10.1016/j.cell.2024.11.027.

39 Taoka T, Ito R, Nakamichi R, Nakane T, Kawai H, Naganawa S. Diffusion tensor image analysis along the perivascular space (DTI-ALPS): revisiting the meaning and significance of the method. *Magn Reson Med Sci*. 2024;23(3):268–290. https://doi.org/10.2463/mrms.rev.2023-0175.

40 Ghaderi S, Mohammadi S, Jouzdani AF, Ahmadzadeh AM, Fatehi F. A systematic review and meta-analysis on glymphatic flow dysfunction in Parkinson's disease and parkinsonism spectrum. *NPJ Parkinsons Dis*. 2025;11(1):306. https://doi.org/10.1038/s41531-025-01151-4.

41 Khalafi M, Shirbandi K, Zhou L, et al. Diffusion tensor imaging along the perivascular space for characterizing cerebral interstitial fluid dynamics in Alzheimer's disease: a systematic review and meta-analysis. *AJNR Am J Neuroradiol*. 2025. https://doi.org/10.3174/ajnr.A8953.

42 Moses J, Sinclair B, Law M, O'Brien TJ, Vivash L. Automated methods for detecting and quantitation of enlarged perivascular spaces on MRI. *J Magn Reson Imaging*. 2023;57(1):11–24. https://doi.org/10.1002/jmri.28369.

43 Ashburner J, Friston KJ. Voxel-based morphometry–the methods. *Neuroimage*. 2000;11(6 Pt 1):805–821. https://doi.org/10.1006/nimg.2000.0582.

44 Jones DK, Griffin LD, Alexander DC, et al. Spatial normalization and averaging of diffusion tensor MRI data sets. *Neuroimage*. 2002;17(2):592–617.

45 Taoka T, Ito R, Nakamichi R, et al. Reproducibility of diffusion tensor image analysis along the perivascular space (DTI-ALPS) for evaluating interstitial fluid diffusivity and glymphatic function: CHanges in Alps index on multiple conditiON acquIsition eXperiment (CHAMONIX) study. *Jpn J Radiol*. 2022;40(2):147–158. https://doi.org/10.1007/s11604-021-01187-5.

46 Ardila K, Munro E, Vega F, et al. *Using machine learning to study the effects of genetic predisposition on brain aging in the UK biobank*. 2023:1–5. https://doi.org/10.1109/ISBI53787.2023.10230714.

47 Taylor LW, Simzer EM, Pimblett C, et al. p-tau Ser356 is associated with Alzheimer's disease pathology and is lowered in brain slice cultures using the NUAK inhibitor WZ4003. *Acta Neuropathol*. 2024;147(1):7. https://doi.org/10.1007/s00401-023-02667-w.

48 Mathiesen BK, Miyakoshi LM, Cederroth CR, et al. Delivery of gene therapy through a cerebrospinal fluid conduit to rescue hearing in adult mice. *Sci Transl Med*. 2023;15(702):eabq3916. https://doi.org/10.1126/scitranslmed.abq3916.

49 Corces MR, Shcherbina A, Kundu S, et al. Single-cell epigenomic analyses implicate candidate causal variants at inherited risk loci for Alzheimer's and Parkinson's diseases. *Nat Genet*. 2020;52(11): 1158–1168. https://doi.org/10.1038/s41588-020-00721-x.

50 Zhao B, Shan Y, Yang Y, et al. Transcriptome-wide association analysis of brain structures yields insights into pleiotropy with complex neuropsychiatric traits. *Nat Commun*. 2021;12(1):2878. https://doi.org/10.1038/s41467-021-23130-y.

51 Zhukovsky P, Tio ES, Coughlan G, et al. Genetic influences on brain and cognitive health and their interactions with cardiovascular conditions and depression. *Nat Commun*. 2024;15(1):5207. https://doi.org/10.1038/s41467-024-49430-7.

52 Hsu HC, Lee YL, Cheng TS, et al. Characterization of two non-testis-specific CABYR variants that bind to GSK3beta with a proline-rich extensin-like domain. *Biochem Biophys Res Commun*. 2005;329(3):1108–1117. https://doi.org/10.1016/j.bbrc.2005.02.089.

53 Simone R, Javad F, Emmett W, et al. MIR-NATs repress MAPT translation and aid proteostasis in neurodegeneration. *Nature*. 2021;594(7861):117–123. https://doi.org/10.1038/s41586-021-03556-6.

54 Srinivas T, Mathias C, Oliveira-Mateos C, Guil S. Roles of lncRNAs in brain development and pathogenesis: emerging therapeutic opportunities. *Mol Ther*. 2023;31(6):1550–1561. https://doi.org/10.1016/j.ymthe.2023.02.008.

55 Liu J. PSMB4: a potential biomarker and therapeutic target for depression, perspective from integration analysis of depression GWAS data and human plasma proteome. *Transl Psychiatry*. 2025;15(1):62. https://doi.org/10.1038/s41398-025-03279-6.

56 Shi J, Liu X, Xu C, et al. Up-regulation of PSMB4 is associated with neuronal apoptosis after neuroinflammation induced by lipopolysaccharide. *J Mol Histol*. 2015;46(6):457–466. https://doi.org/10.1007/s10735-015-9637-0.

57 Echaniz-Laguna A, Lornage X, Laforêt P, et al. A new glycogen storage disease caused by a dominant PYGM mutation. *Ann Neurol*. 2020;88(2):274–282. https://doi.org/10.1002/ana.25771.

58 Wang T, Zhou YQ, Wang Y, et al. Long-term potentiation-based screening identifies neuronal PYGM as a synaptic plasticity regulator participating in Alzheimer's disease. *Zool Res*. 2023;44(5):867–881. https://doi.org/10.24272/j.issn.2095-8137.2023.123.

59 Zelko IN, Mariani TJ, Folz RJ. Superoxide dismutase multigene family: a comparison of the CuZn-SOD (SOD1), Mn-SOD (SOD2), and EC-SOD (SOD3) gene structures, evolution, and expression. *Free Radic Biol Med*. 2002;33(3):337–349. https://doi.org/10.1016/s0891-5849(02)00905-x.

60 Mai N, Miller-Rhodes K, Prifti V, Kim M, O'Reilly MA, Halterman MW. Lung-Derived SOD3 attenuates neurovascular injury after transient global cerebral ischemia. *J Am Heart Assoc*. 2019;8(9):e011801. https://doi.org/10.1161/jaha.118.011801.

61 Tian S, Hong H, Luo X, Zeng Q, Huang P, Zhang M. Association between body mass index and glymphatic function using diffusion tensor image-along the perivascular space (DTI-ALPS) in patients with Parkinson's disease. *Quant Imaging Med Surg*. 2024;14(3):2296–2308. https://doi.org/10.21037/qims-23-1032.

62 Peila R, Rohan TE. The association between the healthy lifestyle index and MRI-derived body composition measurements in the UK Biobank study. *Sci Rep*. 2025;15(1):1010. https://doi.org/10.1038/s41598-024-84406-z.

63 Carotenuto A, Cacciaguerra L, Pagani E, Preziosa P, Filippi M, Rocca MA. Glymphatic system impairment in multiple sclerosis: relation with brain damage and disability. *Brain*. 2022;145(8): 2785–2795. https://doi.org/10.1093/brain/awab454.

64 Bao W, Jiang P, Xu P, et al. Lower DTI-ALPS index in patients with major depressive disorder: correlation with fatigue. *Behav Brain Res*. 2025;478:115323. https://doi.org/10.1016/j.bbr.2024.115323.

65 Zhang C, Sha J, Cai L, et al. Evaluation of the glymphatic system using the DTI-ALPS index in patients with spontaneous intracerebral haemorrhage. *Oxid Med Cell Longev*. 2022;2022:2694316. https://doi.org/10.1155/2022/2694316.

66 Stahl SM. Mechanism of action of serotonin selective reuptake inhibitors. Serotonin receptors and pathways mediate therapeutic effects and side effects. *J Affect Disord*. 1998;51(3):215–235. https://doi.org/10.1016/s0165-0327(98)00221-3.

67 Du W, Chen H, Gróf I, et al. Antidepressant-induced membrane trafficking regulates blood-brain barrier permeability. *Mol Psychiatry*. 2024;29(11):3590–3598. https://doi.org/10.1038/s41380-024-02626-1.

68 Medina-Rodriguez EM, Beurel E. Blood brain barrier and inflammation in depression. *Neurobiol Dis*. 2022;175:105926. https://doi.org/10.1016/j.nbd.2022.105926.

69 Passero S, Nardini M, Battistini N. Regional cerebral blood flow changes following chronic administration of antidepressant drugs. *Prog Neuropsychopharmacol Biol Psychiatry*. 1995;19(4):627–636. https://doi.org/10.1016/0278-5846(95)00107-7.

70 Wichniak A, Wierzbicka A, Jernajczyk W. Sleep and antidepressant treatment. *Curr Pharm Des*. 2012;18(36):5802–5817. https://doi.org/10.2174/138161212803523608.

71 Anagha K, Shihabudheen P, Uvais NA. Side effect profiles of selective serotonin reuptake inhibitors: a cross-sectional study in a naturalistic setting. *Prim Care Companion CNS Disord*. 2021;23(4):20m02747. https://doi.org/10.4088/PCC.20m02747.

72 Saha K, Torous J, Kiciman E, De Choudhury M. Understanding side effects of antidepressants: large-scale longitudinal study on social media data. *JMIR Ment Health*. 2021;8(3):e26589. https://doi.org/10.2196/26589.